Automatica 135 (2022) 109977

Contents lists available at ScienceDirect

Automatica

journal homepage: www.elsevier.com/locate/automatica

Brief paper

Dynamic inversion-based hysteresis compensation using extended high-gain observer☆

Dhrubajit Chowdhury *, Yasir K. Al-Nadawi, Xiaobo Tan

Department of Electrical and Computer Engineering, Michigan State University, East Lansing, 48824, USA

ARTICLE INFO

Article history:
Received 21 July 2019
Received in revised form 16 July 2021
Accepted 4 August 2021
Available online 8 November 2021

Keywords:
Dynamic inversion
Extended high-gain observer
Hysteresis
Smart materials
Tracking

ABSTRACT

We consider the tracking problem for an uncertain nonlinear single-input-single-output system satisfying the minimum-phase assumption, preceded by an unknown hysteresis operator. This is a widely used model for smart material-actuated systems, such as piezo-based nanopositioning systems. Existing hysteresis compensation methods typically require explicit hysteresis models, which tend to be high-dimensional operators and entail significant complexity in model identification and inversion. We propose an output feedback-based hysteresis compensation approach for this class of systems using dynamic inversion and extended high-gain observers. With mild assumptions on the hysteresis nonlinearity properties, the system can be represented as an uncertain, nonaffine, nonlinear system containing a hysteretic perturbation. Dynamic inversion is used to deal with the nonaffine input, uncertainties, and the hysteretic perturbation, where the latter two are estimated using an extended high-gain observer. Analysis of the closed-loop system under output feedback shows that the tracking error converges to a small neighborhood near the origin, which can be made arbitrarily small via a proper choice of time-scale parameters of dynamic inversion and the observer, respectively. Simulation results are presented to show the interplay between these two parameters. Finally, experiments conducted on a commercial nanopositioner confirm the theoretical analysis and demonstrate that the proposed method delivers performance comparable to several competing methods, all of which require an explicit hysteresis inversion operator.

1. Introduction

Smart materials are being increasingly used in sensing and actuation applications due to their compact size and large bandwidth of operation, e.g., nanopositioning (Esbrook, Tan, & Khalil, 2013). However, smart materials are widely known to exhibit the hysteresis phenomenon (Bertotti & Mayergoyz, 2006), which affects positioning precision as it becomes challenging to control the system (Tao & Kokotovic, 1995) and, if not compensated, causes degraded tracking performance. Consequently, there has been significant research interest in hysteresis modeling, and control design techniques (Devasia, Eleftheriou, & Moheimani, 2007) to mitigate its effect.

Hysteresis models can be mainly classified into physics-based and phenomenology-based models. The physics-based models are system-dependent and focus on the first principles of physics, while the phenomenology-based models aim to replicate the natural behavior of the system without giving insight into the physics of the system. Since they are not specific to a physical system, these models are generally applicable to a large class of hysteretic systems. Examples of these mathematical models, also widely known as hysteresis operators, include the Preisach operator (Mayergoyz, 2003), Tan and Baras (2004), Prandtl–Ishlinskii (PI) operator (Brokate & Sprekels, 2012), Preisach–Krasnosel'skii–Pokrovskii (PKP) operator (Krasnosel'skiĭ & Pokrovskiĭ, 1989), Duhem model (Oh & Bernstein, 2005) and Bouc–Wen model (Bouc, 1967).

A predominant control approach to mitigating the hysteresis effect is to use feedforward compensation (Leang, Zou, & Devasia, 2009), which approximately cancels the hysteresis effect by identifying a hysteresis model and then constructing an inverse hysteresis operator. However, some operators, like the Preisach operator, do not admit an analytical form of its inverse, and therefore computation-intensive recursive techniques need to be used (Ruderman & Rachinskii, 2018; Tan & Baras, 2004). For operators like the finite-dimensional classical (Krejci & Kuhnen, 2001), modified (Kuhnen, 2003), and generalized PI operators (Janaideh, Rakheja, & Su, 2011) where analytical formulas exist, the number

☆ This work was supported in part by National Science Foundation, United States (CMMI 1301243). The material in this paper was presented at the ASME Dynamic Systems and Control Conference, September 30-October 3, 2018, Atlanta, Georgia, USA. This paper was recommended for publication in revised form by Associate Editor Zhihua Qu under the direction of Editor Daniel Liberzon.

* Corresponding author.
E-mail addresses: chowdh48@msu.edu (D. Chowdhury), alnadawi@msu.edu (Y.K. Al-Nadawi), xbtan@msu.edu (X. Tan).

https://doi.org/10.1016/j.automatica.2021.109977
0005-1098/

of hysterons needs to be sufficiently high to have adequate model accuracy, which entails more storage space and computational effort. Finally, due to the multi-valued and non-smooth feature of hysteresis, the identified parameters of these hysteresis models exhibit strong sensitivity to unknown measurement errors (Wang & Su, 2006).

The feedforward compensation is often open-loop in nature, which leads to tracking performance degradation due to inversion error, model uncertainties, and environmental changes. Therefore, advanced feedback control techniques are typically integrated with the inverse hysteresis operator to compensate for uncertainties in the system. Adaptive control is one approach used to deal with the inversion error that arises due to uncertainty in the hysteresis parameters (Chen, Hisayama, & Su, 2010; Tao & Kokotovic, 1995; Wang & Su, 2006). Another approach is to consider the inversion error as an unknown disturbance and employ the proportional–integral controller to deal with it, but this approach fails to track well at high frequencies (Bashash & Jalili, 2009). More advanced techniques, such as sliding-mode control, which use knowledge of the bound on the inversion error, are robust against disturbances and parametric uncertainties (Edardar, Tan, & Khalil, 2015). In Ruderman and Bertram (2010), a Discrete Dynamic Preisach model was developed to compute the Preisach operator and its inverse. To improve the performance against uncertainty, the algorithm uses the error signal between the estimated hysteresis output and the true hysteresis output.

Inversion-free and implicit-inversion-based hysteresis compensation approaches do not require the modeling and extensive computation effort as in explicit hysteresis inversion approaches and therefore are of interest. An inversion-free robust adaptive control approach is used in Wang and Su (2006) for plants with known nonlinearity cascaded with the PI operator, which can be decomposed into a combination of a linear term and a bounded hysteretic perturbation. Other adaptive controller approaches are based on pseudo inversion (Chen, Hisayama, & Su, 2009) and implicit inversion (Chen et al., 2010). Another alternative approach to hysteresis compensation that does not involve explicit inversion is based on observers; see Goforth and Gao (2008), Yi, Chang, and Shen (2009), Al Janaideh and Boker (2018) where a linear system preceded by a hysteresis nonlinearity is considered. These approaches follow the same idea of Wang and Su (2006) for decomposing the hysteresis operator. However, unlike (Wang & Su, 2006), where the hysteretic perturbation (disturbance) is dominated using a robust controller, in these approaches, it is estimated via an observer and then subsequently canceled (approximately) through feedback control. In comparison to these approaches, we have three major differences: (i) compared to a linear system preceded by a hysteresis operator, we consider a nonlinear system defined in the normal form cascaded with a hysteretic operator; (ii) we consider the control input to be nonaffine compared to the affine control input assumed in the above-mentioned approaches; (iii) we use dynamic inversion combined with an extended high-gain observer which compensates for the hysteresis and achieves closed-loop tracking.

In this paper, with mild assumptions on the general properties of the hysteresis, we apply dynamic-inversion (Hovakimyan, Lavretsky, & Sasane, 2007), to effectively compute the hysteresis inverse without requiring an explicit model of the hysteresis. In order to implement the dynamic inversion algorithm, an extended high-gain observer (Freidovich & Khalil, 2008) is used to estimate the hysteretic part, system states, and uncertainties at a time scale faster than the plant dynamics and the dynamic inversion. While an extended high-gain observer has been used with dynamic inversion in Lee, Mukherjee, and Khalil (2016) for memory-less nonaffine nonlinearities, we believe that the proposed approach is the first attempt to deal with a nonaffine hysteretic nonlinearity using dynamic inversion and an extended high-gain observer. The proposed algorithm presents several advantages over other inversion-free approaches in the literature. Firstly, the non-hysteretic component is assumed to be general with a mild assumption, unlike the other inversion-free approaches (Chen et al., 2010; Chen, Ren, & Zhong, 2015), in literature, which assumes that the non-hysteretic component to be linear. Secondly, the plant is considered to be nonlinear, satisfying the minimum-phase assumption. Thirdly, the proposed controller's computation time is invariant with respect to the complexity of the underlying hysteresis operator. This is in contrast to inversion-based approaches, where the controller computation time typically increases with the number of hysteretic elements in the model.

We compare the proposed method with several competing methods proposed by our group, including the sliding mode controller (SMC) (Edardar et al., 2015), single harmonic servocompensator (SHSC) (Esbrook et al., 2013) and the multiple harmonic servocompensator (MSHC) (Esbrook et al., 2013), all of which use an explicit hysteresis inversion operator. Selecting these robust control techniques for comparison is mainly because of the following reasons: (i) The aforementioned approaches are comparable to our approach in the sense that they are robust control algorithms. (ii) All these approaches are implemented with an inverse operator inserted at the input side. Therefore, obtaining comparable or better results shows the efficacy of the proposed controller, which is simpler in structure compared to these approaches. (iii) The compared approaches were implemented on the same apparatus under comparable experimental conditions, which makes the comparison fair when evaluating the methods.

A preliminary version of this paper was presented at the 2018 ASME Dynamic Systems, and Control Conference (Chowdhury, Al-Nadawi, & Tan, 2018). The enhancements of this paper over (Chowdhury et al., 2018) include (1) rigorous analysis of the closed-loop system behavior under the output feedback controller, (2) more extensive simulation results exploring the roles of time-scale parameters, (3) experimental validation of the proposed approach with a nanopositioner, and (4) comparison of the proposed controller with several explicit hysteresis inversion-based methods.

2. Problem formulation

The plant dynamics is given by

$$\dot{\eta} = f_0(\eta, \xi, w), \tag{1a}$$

$$\dot{\xi} = A\xi + B[f(\eta, \xi, w) + \Upsilon(t)], \tag{1b}$$

$$\Upsilon(t) = \Gamma\left[u(\tau)|_{\tau=0}^{t}, H_0\right](t), \tag{1c}$$

$$y = \xi_1, \tag{1d}$$

which is a single-input-single-output system defined in the normal form (Khalil, 2002), with a hysteretic operator at the input side. The pair (A, B) represents a chain of ρ integrators. The matrices $A \in \mathbb{R}^{\rho\times\rho}$ and $B \in \mathbb{R}^{\rho\times 1}$ are defined as

$$A = \begin{bmatrix} 0 & 1 & 0 & \dots & 0 \\ 0 & 0 & 1 & \dots & 0 \\ \vdots & \vdots & \ddots & \ddots & \vdots \\ 0 & 0 & \dots & 0 & 1 \\ 0 & 0 & \dots & \dots & 0 \end{bmatrix}, \quad B = \begin{bmatrix} 0 \\ 0 \\ \vdots \\ 0 \\ 1 \end{bmatrix}.$$

The functions f and f_0 depend on the variables η, ξ, w and satisfy Assumption 2. The variable $\eta \in \mathbb{R}^{n-\rho}$ is the internal state, $\xi = \text{col}(\xi_1, \dots, \xi_\rho) \in \mathbb{R}^\rho$ is the external state, $u \in \mathbb{R}$ is the control input, and $y \in \mathbb{R}$ is the output of the system, $\Gamma[\cdot, \cdot]$

is a hysteresis operator, $\Upsilon \in \mathbb{R}$ is the output of the hysteresis operator, which depends on the history of the input $u(\tau)|_{\tau=0}^{t}$ and the initial internal state H_0 of the operator Γ, $w \in \mathbb{R}^l$ is an exogenous input and ρ is the relative degree of the system. The normal form is defined for $\eta \in D_\eta \subset \mathbb{R}^{n-\rho}$ and $\xi \in D_\xi \subset \mathbb{R}^\rho$ for some domains D_η and D_ξ. The system is required to satisfy the following assumptions.

Assumption 1. For any given t, $w(t)$ and $\dot{w}(t)$ are bounded, and $w(t)$ belongs to a known compact set $W \subset \mathbb{R}^l$.

Assumption 2. The function f is continuously differentiable with locally Lipschitz derivatives and f_0 is locally Lipschitz for all $(\eta, \xi, w) \in D_\eta \times D_\xi \times W$.

Assumption 3. There exist a continuously differentiable function $V_0(\eta)$, class $\mathcal{K}_\infty$ functions Ψ_1, Ψ_2, and $\mathcal{K}$ function Ψ_3, such that

$$\Psi_1(\|\eta\|) \le V_0(\eta) \le \Psi_2(\|\eta\|), \tag{2a}$$

$$\frac{\partial V_0}{\partial \eta} f_0(\eta, \xi, w) \le 0, \ \text{ for } \|\eta\| \ge \Psi_3(\|\xi\| + \|w\|), \tag{2b}$$

for all $(\eta, \xi, w) \in D_\eta \times D_\xi \times W$.

Assumption 3 implies that the internal dynamics of the system is regionally input-to-state stable.

Assumption 4. The hysteresis operator Γ can be decomposed as

$$\Gamma\left[u(\tau)|_{\tau=0}^{t}, H_0\right](t) = g(u(t)) + \tilde{\Gamma}\left[u(\tau)|_{\tau=0}^{t}, H_0\right](t), \tag{3}$$

for some non-hysteretic function $g(\cdot)$ and remaining hysteretic term $\tilde{\Gamma}$, and

(i) $g(\cdot)$ is continuously differentiable and satisfies

$$\beta_1 \le \frac{\mathrm{d}g(u)}{\mathrm{d}u} \le \beta_2, \tag{4}$$

where β_1 and β_2 are positive constants with $\beta_2 \ge \beta_1$.

(ii) $\tilde{\Gamma}$ is a bounded, monotone hysteresis operator in the sense that

$$\begin{aligned} 0 &\le (u_1(t) - u_2(t))(\tilde{\Gamma}[u_1(\tau)|_{\tau=0}^{t}, H_0](t) - \tilde{\Gamma}[u_2(\tau)|_{\tau=0}^{t}, H_0](t)) \\ &\le k(u_1(t) - u_2(t))^2, \end{aligned} \tag{5}$$

where $u_1(\tau)|_{\tau=0}^{t}$ and $u_2(\tau)|_{\tau=0}^{t}$ are both monotonically increasing (or decreasing) inputs with $u_1(0) = u_2(0)$, and k is a positive constant. In addition, $\tilde{\Gamma}[u(\tau)|_{\tau=0}^{t}, H_0](t)$ is piecewise continuously differentiable with respect to $u(t)$ for a monotonic function u, which, along with (5), implies

$$0 \le \frac{\partial \tilde{\Gamma}[u(\tau)|_{\tau=0}^{t}, H_0](t)}{\partial u(t)} \le k. \tag{6}$$

Remark 1. Assumption 4 is satisfied by a wide class of hysteresis operators, including the classical PI operator, the generalized PI operator, and the Preisach operator. For example, for a classical PI operator with $N+1$ plays, the hysteresis output is given by

$$\Upsilon(t) = \theta_0 u(t) + \tilde{\Gamma}[u(\tau)|_{\tau=0}^{t}, H_0], \tag{7}$$

where

$$\tilde{\Gamma}[u(\tau)|_{\tau=0}^{t}, H_0] = \sum_{i=1}^{N} \theta_i \Gamma_{r_i}\left[u(\tau)|_{\tau=0}^{t}, H_0\right](t).$$

The variable θ_i is the weight associated with play Γ_{r_i} with threshold r_i, θ_0 is the weight associated with the play with threshold $r_i = 0$ (the memory-less term), and H_0 represents the vector of initial values of all plays. The classical PI operator satisfies Eq. (6). It can be shown that when $\Gamma_{r_i}\left[u(\tau)|_{\tau=0}^{t}, H_0\right](t)$ is in the play or linear region, then

$$0 \le \frac{\partial \tilde{\Gamma}[u(\tau)|_{\tau=0}^{t}, H_0]}{\partial u(t)} \le \sum_{i=1}^{N} \theta_i.$$

If $\theta_0 > 0$ and $\theta_i \ge 0$ for $i = 1, 2, \ldots, N$, the classical PI model satisfies all conditions in Assumption 4. Similarly, a generalized PI model satisfies Assumption 4 if the non-hysteretic component satisfies (4) and all generalized plays have non-negative weights.

Remark 2. Assumption 4 is also satisfied by Preisach-like operators (where the basic building block is a variant of the Preisach hysteron), such as the Krasnosel'skii–Pokrovskii (KP) operator. This operator has been used for hysteresis modeling in smart materials, e.g., shape memory alloy (SMA) actuators (Webb, Lagoudas, & Kurdila, 1998). The output of a KP model is given by

$$\Upsilon(t) = g(u) + \Gamma[u(\tau)_{\tau=0}^{t}, H_0](t),$$

where $g(u)$ satisfies (4) and $\Gamma[\cdot]$ consists of KP hysterons which are the same as that of a play operator, when it is unsaturated, namely, when its output is within the interval $(-1, 1)$.

Property 1. *For hysteresis operator Γ satisfying Assumption 4, one can show,*

(i) Γ admits a unique (right) inverse, denoted as Γ^{-1}, in the sense that, $\Gamma \circ \Gamma^{-1} = I$ (identity), i.e., $\Gamma[\Gamma^{-1}[\Upsilon(\tau)|_{\tau=0}^{t}, H_0^-], H_0](t) = \Upsilon(t)$, for any continuous and monotone function Υ, where H_0^- is the corresponding initial condition of Γ^{-1}.

(ii) For a continuous monotonic input $\Upsilon(t)$,

$$\frac{1}{\beta_2 + k} \le \frac{\partial\ \Gamma^{-1}[\Upsilon(\tau)|_{\tau=0}^{t}, H_0^-](t)}{\partial \Upsilon(t)} \le \frac{1}{\beta_1}. \tag{8}$$

The derivative exists except possibly for a discrete number of points. Moreover, for any compact time interval, the jumps of the derivative of $\Gamma^{-1}[\Upsilon(\tau)|_{\tau=0}^{t}, H_0^-](t)$ will be bounded and this follows from (8).

Remark 3. Eq. (8) shows that the slope of any segment on the hysteresis graph (u vs. Υ) for Γ^{-1} is bounded between two positive constants, $1/(\beta_2 + k)$ and $1/\beta_1$.

Assumption 5. The reference signal $r(t)$ and its derivatives up to $r^{(\rho+1)}(t)$ are bounded for all $t \ge 0$. Moreover, $\mathcal{R}(t) = \mathrm{col}(r(t), r^{(1)}(t), \ldots, r^{(\rho-1)}(t)) \in D_\xi$ for all $t \ge 0$

The tracking objective is satisfied when the output y of the plant (1) tracks the reference signal r. The change of variables

$$e_1 = \xi_1 - r(t), \quad e_2 = \xi_2 - r^{(1)}(t), \ \ldots, \ e_\rho = \xi_\rho - r^{(\rho-1)}(t), \tag{9}$$

transforms the system (1a)–(1d) into the form

$$\dot{\eta} = f_0(\eta, e + \mathcal{R}, w), \tag{10a}$$

$$\dot{e} = Ae + B\left\{F\left(\eta, e, \mathcal{R}, w, r^{(\rho)}\right) + \Gamma[u](t)\right\}, \tag{10b}$$

$$e_1 = y - r, \tag{10c}$$

where

$$F\left(\eta, e, \mathcal{R}, w, r^{(\rho)}\right) = f(\eta, e + \mathcal{R}, w) - r^{(\rho)}, \tag{11}$$

and $e = \mathrm{col}(e_1, e_2, \ldots, e_\rho)$. For ease of notation, we have dropped the initial condition from the hysteresis operator argument, and for simplicity, we write the hysteresis output as $\Gamma[u](t)$. Similarly, we drop t from the definition of the reference signal and its derivatives.

3. State feedback controller

In this section, we design the state feedback controller in preparation for the discussion of the output feedback controller. The section includes the definitions of all the compact sets in which the closed-loop analysis is carried out. Furthermore, we also show the stability of the closed-loop system under the state feedback controller.

In this paper the dynamic inversion controller u needs to be designed such that the closed-loop system behaves as

$$\dot{e} = (A - BK)e, \tag{12}$$

where K is chosen such that the matrix $(A - BK)$ is Hurwitz. Let $V_e(e) = e^T P e$, where P is the solution to the Lyapunov equation $P(A - BK) + (A - BK)^T P = -Q$, for some positive-definite symmetric matrix Q. Let c be a positive constant and define $\Omega_c = \{e : V_e(e) \leq c\}$. Choose $c > 0$ such that for every $e \in \Omega_c$, $\xi = e + \mathcal{R} \in D_\xi$ and therefore $\{\xi : V_e(e) \leq c\} \subset D_\xi$. Next we define the set $\Omega_0 = \{\eta : V_0(\eta) \leq c_0\}$, which is compact and contained in D_η, where c_0 is chosen such that $c_0 \geq \Psi_2(\Psi_3(\kappa_1(c) + \kappa_2 + \kappa_3))$, where $\kappa_1(c) = \max_{e \in \Omega_c} \|e\|$, $\kappa_2 = \max_{w \in W} \|w\|$, and $\kappa_3 = \max_t \|\mathcal{R}(t)\|$. From Assumption 3, the set $\Omega_0 \times \Omega_c$ is positively invariant with respect to the system

$$\dot{\eta} = f_0(\eta, e + \mathcal{R}, w), \quad \dot{e} = (A - BK)e,$$

because on the boundary $\{\eta : V_0(\eta) = c_0\}$,

$$\begin{aligned} &\Psi_2(\|\eta\|) \geq c_0 \geq \Psi_2(\Psi_3(\kappa_1(c) + \kappa_2 + \kappa_3)), \\ \implies &\|\eta\| \geq \Psi_3(\kappa_1(c) + \kappa_2 + \kappa_3), \\ \implies &\|\eta\| \geq \Psi_3(\|\xi\| + \|w\|) \implies \dot{V}_0 \leq 0, \end{aligned}$$

and on the boundary $\{e : V_e(e) = c\}$, $\dot{V}_e < 0$.

The state feedback controller is designed by assuming perfect knowledge of the function $f(\cdot)$, states (η, ξ), exogenous input w, the reference signal and its derivatives, and the hysteresis output $\Gamma[u](t)$. The analysis of the state feedback case determines the saturation level that will be used in output feedback controller design. The saturation levels can be chosen from the closed-loop system simulation under the state feedback controller to see the maximum value of the signals. Therefore, in order to determine the saturation levels, some rudimentary knowledge about the system is required as the state feedback case can be simulated using a nominal system model. In the output feedback section, we will require the knowledge of the tracking error $e_1(t)$ and the compact sets Ω_0, Ω_c, Ω_z, W, R_0 and R_1 to determine the saturation levels. R_0 and R_1 are defined later in this section. The observer is used to estimate the signals $e_2, \ldots, e_\rho$ and the term $\sigma(t) = F(\eta(t), e(t), \mathcal{R}, w(t), r^{(\rho)}(t)) + \Gamma[u](t)$.

The dynamic inversion algorithm is then given by

$$\mu \dot{u} = -\left[F\left(\eta, e, \mathcal{R}, w, r^{(\rho)}\right) + \Gamma[u](t) + Ke\right], \tag{13}$$

where μ is a small positive constant and F is defined in (11). The quasi-steady state is obtained by setting $\mu = 0$,

$$f(\eta, e + \mathcal{R}, w) + \Gamma[u](t) - r^{(\rho)} = -Ke. \tag{14}$$

From Assumption 5, $r^{(\rho)}$ and $r^{(\rho+1)}$ are bounded. Let $d_1 = \max_t |r^{(\rho)}(t)|$ and $d_2 = \max_t |r^{(\rho+1)}(t)|$. Define the sets $R_0 = \{\mathcal{R} : \|\mathcal{R}\| \leq \kappa_3\}$, $R_1 = \{r^{(\rho)} : |r^{(\rho)}| \leq d_1\}$, and $R_2 = \{r^{(\rho+1)} : |r^{(\rho+1)}| \leq d_2\}$. From Property 1, if $(\eta, e, \mathcal{R}, w, r^{(\rho)}) \in \Omega_0 \times \Omega_c \times R_0 \times W \times R_1$ for each $\tau \in [0, t]$, Eq. (14) has a unique solution given by

$$u^*(t) = \phi[\chi](t) \triangleq \Gamma^{-1}\left[\chi(\tau)|_{\tau=0}^t\right](t),$$

where

$$\chi(\tau) = -f(\eta(\tau), e(\tau) + \mathcal{R}(\tau), w(\tau)) + r^{(\rho)}(\tau) - Ke(\tau),$$

and Γ^{-1} is the inverse of the hysteresis operator Γ. Furthermore, from Assumption 1, 2, and 5, χ is continuously differentiable with respect to t. The change of variables

$$z(t) = u(t) - \phi[\chi](t),$$

transforms system (13) and (10b) into

$$\dot{e} = (A - BK)e + B\{\Gamma[z + \phi] - \Gamma[\phi]\}, \tag{15a}$$

$$\mu \dot{z} = -(\Gamma[z + \phi] - \Gamma[\phi]) - \mu \dot{\phi}, \tag{15b}$$

where

$$\dot{\phi} = \frac{\partial}{\partial \chi(t)}\left(\Gamma^{-1}\left[\chi(\tau)|_{\tau=0}^t\right]\right)\dot{\chi}(t).$$

Note that $\dot{\chi}(t)$ is bounded for all $(\eta, e, \mathcal{R}, w, r^{(\rho)}, r^{(\rho+1)}) \in \Omega_0 \times \Omega_c \times R_0 \times W \times R_1 \times R_2$. From Property 1, it follows that $\frac{\partial}{\partial \chi(t)}\left(\Gamma^{-1}\left[\chi(\tau)|_{\tau=0}^t\right]\right)$ is bounded for all $(\eta, e, \mathcal{R}, w, r^{(\rho)}) \in \Omega_0 \times \Omega_c \times R_0 \times W \times R_1$, from which we can conclude that $\dot{\phi}$ is bounded for all $(\eta, e, \mathcal{R}, w, r^{(\rho)}, r^{(\rho+1)}) \in \Omega_0 \times \Omega_c \times R_0 \times W \times R_1 \times R_2$.

Let $|u| \leq q_0$, where q_0 is a positive constant, and we define the compact set $\Omega_z = \{z : |z| \leq q\}$, where

$$q \geq q_0 + \max_{(\eta, e, \mathcal{R}, w, r^{(\rho)}) \in \Omega_0 \times \Omega_c \times R_0 \times W \times R_1} |\phi|.$$

The right-hand side of (15b) using Property 1 is bounded for all $(\eta, e, z, \mathcal{R}, w, r^{(\rho)}, r^{(\rho+1)}) \in \Omega_0 \times \Omega_c \times \Omega_z \times R_0 \times W \times R_1 \times R_2$. The solution of (15b) is therefore studied in the sense of Filippov solution (Filippov, 2013), which satisfies

$$z(t) = z(0) - \frac{1}{\mu}\int_0^t [\Gamma[z(\tau) + \phi(\tau)] - \Gamma[\phi(\tau)] - \mu E_1(\tau)] d\tau,$$

where $E_1(t) \in K_c\{\dot{\phi}(t)\}$ for almost all t and the convex hull $K_c\{\dot{\phi}(t)\}$ is defined in Filippov (Filippov, 2013). Similar to Oh and Khalil (1995), Theorem 1 of Paden and Sastry (1987) is used for the calculus of Filippov's differential inclusion.

Theorem 1. *Consider the closed-loop system formed of the plant (10) and the dynamic inversion algorithm (13). Suppose that Assumptions 1–5 are satisfied and $(\eta(0), e(0))$ belongs to a known compact subset in the interior of $\Omega_0 \times \Omega_c$, $|z(0)| < q$. Then there exists $\mu^* > 0$ such that for all $\mu \in (0, \mu^*)$, the trajectories of the closed-loop system are bounded for all $t \geq 0$, and*

$$\limsup_{t \to \infty} e(t) = O(\mu), \quad \limsup_{t \to \infty} z(t) = O(\mu). \tag{16}$$

Proof. Consider the Lyapunov functions $V_e = e^T P e$ and $V_z = \frac{1}{2}z^2$. Since $(\eta(0), e(0))$ lie in the interior of the set $\Omega_0 \times \Omega_c$, there exists time $\hat{T}_1 > 0$, such that $|\dot{\phi}| \leq b$, for some positive constant b independent of μ. Therefore, taking the time derivative of V_z along (15b) yields

$$\mu \dot{V}_z \leq -z(\Gamma[z + \phi](t) - \Gamma[\phi](t)) + \mu b|z|.$$

From Eq. (3), $z(\Gamma[z + \phi](t) - \Gamma[\phi](t))$ is equal to

$$z[g(z + \phi) - g(\phi)] + z\left[\tilde{\Gamma}[z + \phi](t) - \tilde{\Gamma}[\phi](t)\right].$$

From Eq. (4), using the mean value theorem (Khalil, 2002), we have

$$\beta_1 z^2 \leq z[g(z + \phi) - g(\phi)] \leq \beta_2 z^2.$$

From Assumption 4, since the hysteresis operator $\tilde{\Gamma}[(\cdot)]$ is monotone, we have

$$z\left[\tilde{\Gamma}[z + \phi](t) - \tilde{\Gamma}[\phi](t)\right] \geq 0.$$

Therefore, we have

$$\dot{V}_z \leq -\frac{\beta_1}{2\mu} z^2, \quad \text{for } |z| \geq \frac{2\mu b}{\beta_1}.$$

It can be shown (Khalil, 2017) that there exists time $\hat{T}_2(\mu) > 0$ where $\lim_{\mu\to 0} \hat{T}_2(\mu) = 0$ such that $|z(t)| \leq b_1\mu$ where $b_1 > 0$ for all $t \in [\hat{T}_2(\mu), \hat{T}_1)$.

Next we analyze the system (15a) for $t \in [\hat{T}_2(\mu), \hat{T}_1)$. Taking the time derivative of V_e along (15a) yields

$$\begin{aligned}\dot{V}_e &= -e^T Qe + 2e^T PB\left(\Gamma[z+\phi](t) - \Gamma[\phi](t)\right),\\ &\leq -\lambda_{\min}(Q)\|e\|^2 + 2\tilde{k}\|e\| \cdot \|PB\| \cdot |z|,\end{aligned}$$

where $\tilde{k} = k + \beta_2$ from (3), (4) and (5), $\lambda_{\max}(Q)$ and $\lambda_{\min}(Q)$ denote the maximum and minimum eigenvalues of the matrix Q, respectively. Since $|z(t)| \leq b_1\mu$ for $t \in [\hat{T}_2(\mu), \hat{T}_1)$, we have

$$\begin{aligned}\dot{V}_e &\leq -\lambda_{\min}(Q)\|e\|^2 + 2\tilde{k}b_1\mu\|PB\| \cdot \|e\|,\\ &\leq -\frac{\lambda_{\min}(Q)}{2}\|e\|^2, \quad \text{for } V_e \geq b_2\mu^2,\end{aligned}$$

where $b_2 = \dfrac{16\tilde{k}^2 b_1^2 \|PB\|^2 \lambda_{\max}(P)}{(\lambda_{\min}(Q))^2}$. Therefore, we can choose $\mu_1 > 0$ such that for all $\mu \in (0, \mu_1)$, the set $\{e : V_e \leq b_2\mu^2\}$ is positively invariant and for sufficiently small μ, the set $\{e : V_e \leq b_2\mu^2\}$ is in the interior of $\{e : V_e \leq c\}$. From which we can conclude that $e(t) \in \Omega_c$ for all $t \geq 0$ and $|z| \leq b_1\mu$ for all $t \geq \hat{T}_2(\mu)$. □

4. Output feedback controller

The implementation of the dynamic inversion algorithm in the previous section requires the knowledge of the function $F(\eta, e, \mathcal{R}, w, r^{(\rho)})$ and the hysteresis output $\Gamma[u](t)$, which is typically not available for use in practice. Therefore, we propose an output feedback controller by combining an extended high-gain observer with the dynamic inversion algorithm to compensate for the hysteresis present in the system. The extended high-gain observer provides an estimate of the combined value at time t for the function F and the hysteresis output Γ, which is then used in the dynamic inversion algorithm. The output feedback controller has two parameters μ and ϵ, which are small and determine the time scales of the dynamic inversion algorithm and the observer, respectively. We set $\sigma(t) = F(\eta(t), e(t), \mathcal{R}, w(t), r^{(\rho)}(t)) + \Gamma[u](t)$. If σ and e were available for feedback, the dynamic inversion algorithm (13) would be given by

$$\mu\dot{u} = -[\sigma + Ke].$$

Since σ and e are not available, we use an extended high-gain observer to get the estimates $(\hat{e}, \hat{\sigma})$ of (e, σ). The extended high-gain observer is constructed as

$$\dot{\hat{e}}_i = \hat{e}_{i+1} + \frac{\alpha_i}{\epsilon^i}(e_1 - \hat{e}_1), \quad 1 \leq i \leq \rho - 1, \tag{17a}$$

$$\dot{\hat{e}}_\rho = \hat{\sigma} + \frac{\alpha_\rho}{\epsilon^\rho}(e_1 - \hat{e}_1), \tag{17b}$$

$$\dot{\hat{\sigma}} = \frac{\alpha_{\rho+1}}{\epsilon^{\rho+1}}(e_1 - \hat{e}_1), \tag{17c}$$

where α_1 to $\alpha_{\rho+1}$ are chosen such that the polynomial

$$s^{\rho+1} + \alpha_1 s^\rho + \cdots + \alpha_{\rho+1} \tag{18}$$

is Hurwitz, and $\epsilon > 0$ is a small parameter. For sufficiently small ϵ, the estimation error decays to zero much faster than the system dynamics. High-gain observer suffers from the peaking phenomenon (Khalil, 2017), where the estimation error peaks to the order of $O(1/\epsilon^\rho)$ during the transient period and then it decays quickly to the order of $O(\epsilon)$. In feedback control the peaking is overcome by designing the control to be a globally bounded function of the estimates $(\hat{e}, \hat{\sigma})$. Let $M > \max_{e\in\Omega_c} |Ke|$, and

$$N > \max_{\substack{(\eta, e, w) \in \Omega_0 \times \Omega_c \times W,\\ \mathcal{R} \in R_0,\ r^{(\rho)} \in R_1,\\ z \in \Omega_z}} |F(\eta, e, \mathcal{R}, w, r^{(\rho)}) + \Gamma[z+\phi]|.$$

The estimates are saturated as $(K\hat{e})_s = M\text{sat}\left(\dfrac{K\hat{e}}{M}\right)$, $\hat{\sigma}_s = N\text{sat}\left(\dfrac{\hat{\sigma}}{N}\right)$, where $\text{sat}(y) = \min\{|y|, 1\}\ \text{sign}(y)$ for $y \in \mathbb{R}$. The dynamic inversion algorithm with the saturated estimates is given by

$$\mu\dot{u} = -[\hat{\sigma}_s + (K\hat{e})_s]. \tag{19}$$

Theorem 2. *Consider the closed-loop system formed of the plant (10), the extended high-gain observer (17), and the dynamic inversion algorithm (19). Suppose that Assumptions 1–5 are satisfied, α_1 to $\alpha_{\rho+1}$ are chosen such that the polynomial (18) is Hurwitz, $(\eta(0), e(0))$ belongs to a known compact subset in the interior of $\Omega_0 \times \Omega_c$, $|z(0)| < q$, and the initial states of the observer belong to a compact subset of $\mathbb{R}^{\rho+1}$. Then there exists $\lambda_1^* > 0$, such that for ϵ and μ with max $\{\mu, \epsilon/\mu\} \leq \lambda_1^*$, the trajectories of the closed-loop system are bounded for all $t \geq 0$, and there exists $T^*(\lambda_1^*) > 0$ such that*

$$\dot{e} = (A - BK)e + O(\lambda_1^*), \quad \forall\ t \geq T^*(\lambda_1^*). \tag{20}$$

Proof. Define the change of variables

$$\begin{aligned}\zeta_i &= (e_i - \hat{e}_i)/\epsilon^{\rho+1-i} \quad \text{for } 1 \leq i \leq \rho,\\ \zeta_{\rho+1} &= \sigma - \hat{\sigma} = f(\eta, e + \mathcal{R}, w) + \Gamma[u](t) - r^{(\rho)} - \hat{\sigma}.\end{aligned}$$

The fast variable dynamics are given by

$$\epsilon\dot{\zeta}_i = -\alpha_i\zeta_1 + \zeta_{i+1} \quad \text{for } 1 \leq i \leq \rho - 1, \tag{22a}$$

$$\epsilon\dot{\zeta}_\rho = -\alpha_\rho\zeta_1 + \zeta_{\rho+1}, \tag{22b}$$

$$\epsilon\dot{\zeta}_{\rho+1} = -\alpha_{\rho+1}\zeta_1 + \epsilon\Delta_0 + (\epsilon/\mu)\Delta_1, \tag{22c}$$

where $\Delta_1 = -\dfrac{\partial\sigma}{\partial u(t)}\Delta_2$,

$$\begin{aligned}\Delta_0 = \frac{\partial\sigma}{\partial\eta}f_0 + \frac{\partial\sigma}{\partial e}\left[(A - BK)e + B\left(\Gamma[z+\phi](t) - \Gamma[\phi](t)\right)\right]\\ + \frac{\partial\sigma}{\partial w}\dot{w} + \frac{\partial\sigma}{\partial\mathcal{R}}\dot{\mathcal{R}} - r^{(\rho+1)},\end{aligned}$$

$$\Delta_2 = \left[\hat{\sigma}_s - \sigma + (K\hat{e})_s - Ke + \Gamma[z+\phi](t) - \Gamma[\phi](t)\right],$$

where the functions f_0, F are written without their arguments. Their complete forms are $f_0 = f_0(\eta, e + \mathcal{R}, w)$ and $F = F(\eta, e, \mathcal{R}, w, r^{(\rho)})$. The term $\dfrac{\partial\sigma}{\partial u(t)}$ can be written as

$$\frac{\partial\sigma}{\partial u(t)} = \frac{\partial\ \Gamma[u(\tau)|_{\tau=0}^t](t)}{\partial u(t)} = \frac{\partial g(u(t))}{\partial u(t)} + \frac{\partial\tilde{\Gamma}[u(\tau)|_{\tau=0}^t](t)}{\partial u(t)}.$$

With Assumption 4, for all $(\eta, e, w, \mathcal{R}, r^{(\rho)}, r^{(\rho+1)}, z) \in \Omega_0 \times \Omega_c \times W \times R_0 \times R_1 \times R_2 \times \Omega_z$, the term $\dfrac{\partial\sigma}{\partial u(t)}$ is bounded. The closed-loop system is represented by

$$\dot{\eta} = f_0(\eta, e + \mathcal{R}, w), \tag{23a}$$

$$\dot{e} = (A - BK)e + B[\Gamma[z+\phi](t) - \Gamma[\phi](t)], \tag{23b}$$

$$\mu\dot{z} = -\left(\Gamma[z+\phi](t) - \Gamma[\phi](t)\right) - \mu\dot{\phi} + \Delta_3, \tag{23c}$$

$$\epsilon\dot{\zeta} = \Lambda\zeta + \epsilon\bar{B}\Delta_0 + (\epsilon/\mu)\bar{B}\Delta_1, \tag{23d}$$

where $\Delta_3 = -\left[\hat{\sigma}_s - \sigma + (K\hat{e})_s - Ke\right]$,
$\zeta = \text{col}(\zeta_1, \ldots, \zeta_{\rho+1})$, and

$$\Lambda = \begin{bmatrix} -\alpha_1 & 1 & 0 & \ldots & 0 \\ -\alpha_2 & 0 & 1 & \ldots & 0 \\ \vdots & \vdots & \ddots & \ddots & \vdots \\ -\alpha_\rho & 0 & \ldots & 0 & 1 \\ -\alpha_{\rho+1} & 0 & \ldots & \ldots & 0 \end{bmatrix}, \quad \bar{B} = \begin{bmatrix} 0 \\ 0 \\ \vdots \\ 0 \\ 1 \end{bmatrix}_{(\rho+1)\times 1}.$$

The solution of (23c)–(23d) is studied in the sense of Filippov solution, which satisfies

$$z(t) = z(0) - \frac{1}{\mu}\int_0^t [\Gamma[z+\phi](\tau) - \Gamma[\phi](\tau) - \mu E_1(\tau) + \Delta_3(\tau)]d\tau, \tag{24a}$$

$$\zeta(t) = \zeta(0) + \frac{1}{\epsilon}\int_0^t [\Lambda\zeta(\tau) + \epsilon\bar{B}\Delta_0(\tau) + (\epsilon/\mu)\bar{B}E_2(\tau)\Delta_2(\tau)]d\tau, \tag{24b}$$

where $E_1(t) \in K_c\{\dot{\phi}(t)\}$ and $E_2(t) \in K_c\{-\frac{\partial\sigma}{\partial u(t)}\}$ for almost all t and the convex hulls are defined in Filippov (Filippov, 2013).

The matrix Λ is Hurwitz by construction. Since the initial states $(\eta(0), e(0), z(0))$ lie in the interior of $\Omega_0 \times \Omega_c \times \Omega_z$ and the right-hand-side functions of Eq. (23a)–(23c) are bounded uniformly in ϵ, there is time $\bar{T} > 0$ such that $(\eta(t), e(t), z(t)) \in \Omega_0 \times \Omega_c \times \Omega_z$ for all $t \in [0, \bar{T}]$. During this time period the terms Δ_0, Δ_1, Δ_2 are bounded by

$$|\Delta_0| \le k_1, \quad |\Delta_1| \le k_2, \quad |\Delta_3| \le k_3,$$

where k_1, k_2, k_3 are positive constants independent of μ and ϵ. This follows from the continuous differentiability of f, local Lipschitz property of f_0, boundedness of $\frac{\partial\sigma}{\partial u(t)}$, and global boundedness of $\hat{\sigma}_s$ and $(K\hat{e})_s$.

We construct the Lyapunov function $V_\zeta = \zeta^T P_0 \zeta$, where $P_0 = P_0^T > 0$ is the solution to the Lyapunov equation $P_0\Lambda + \Lambda^T P_0 = -I$. By taking its time derivative along Eq. (23d) yields

$$\begin{aligned} \epsilon\dot{V}_\zeta &\le -\zeta^T\zeta + 2\epsilon\zeta^T P_0\bar{B}\Delta_0 + 2(\epsilon/\mu)\zeta^T P_0\bar{B}k_2, \\ \epsilon\dot{V}_\zeta &\le -\|\zeta\|^2 + 2\epsilon\|P_0\bar{B}\|\left(k_1 + \frac{k_2}{\mu}\right)\|\zeta\|, \\ \implies \epsilon\dot{V}_\zeta &\le -\frac{1}{2}\|\zeta\|^2, \quad \text{for } V_\zeta \ge \gamma_2(\epsilon/\mu)^2, \end{aligned}$$

where $\gamma_2 = 16\|P_0\bar{B}\|^2\lambda_{\max}(P_0)(k_1+k_2)^2$, $\lambda_{\max}(P_0)$ is the maximum eigenvalue of P_0. Following the high gain observer theory (Lee et al., 2016), one can show that $\|\zeta(t)\| \le \tilde{\gamma}_2(\epsilon/\mu)$ where $\tilde{\gamma}_2 > 0$ for time $t \ge T_1(\epsilon)$, where $\lim_{\epsilon\to 0} T_1(\epsilon) = 0$. For sufficiently small ϵ, $T_1(\epsilon) < (1/2)\bar{T}$. Therefore, for $t \in [T_1(\epsilon), \bar{T})$, $\|\zeta(t)\| \le \tilde{\gamma}_2(\epsilon/\mu)$ and $(\eta(t), e(t), z(t))$ remains in the set $\Omega_0 \times \Omega_c \times \Omega_z$. For $\|\zeta(t)\| \le \tilde{\gamma}_2(\epsilon/\mu)$, we have

$$K\hat{e} = Ke + O(\lambda), \quad \hat{\sigma} = \sigma + O(\lambda).$$

Therefore, for sufficiently small λ, where $\lambda = \max\left\{\frac{\epsilon}{\mu}, \mu\right\}$, we have $K\hat{e} < M$ and $\hat{\sigma} < N$ which implies that the saturation in the estimates is no longer active, hence $K\hat{e}_s = K\hat{e}$, $\hat{\sigma}_s = \hat{\sigma}$.

Next we analyze the system (23c) for $t \in [T_1(\epsilon), \bar{T})$. Note that $z(t) \in \Omega_z$ during the time period $[0, T_1(\epsilon)]$. We construct the Lyapunov function $V_z = \frac{1}{2}z^2$ and take its time derivative along Eq. (23c), from which we have

$$\mu\dot{V}_z \le -z\{\Gamma[z+\phi](t) - \Gamma[\phi](t)\} + z\Delta_3 + \mu b|z|.$$

The term Δ_3 during time $t \in [T_1(\epsilon), \bar{T})$ is bounded by $\|\Delta_3\| \le k_4\|\zeta\|$, where k_4 is a positive constant independent of λ, from which we have

$$\begin{aligned} \mu\dot{V}_z &\le -\beta_1 z^2 + \lambda k_5|z|, \\ \implies \mu\dot{V}_z &\le -\frac{\beta_1}{2}|z|^2, \quad \text{for } |z| \ge \gamma_1\lambda, \end{aligned}$$

where k_5 is a positive constant independent of λ and $\gamma_1 = 2k_5/\beta_1$. Similarly, following Lee et al. (2016), one can show that there exists time $T_2(\mu) > 0$ where $\lim_{\mu\to 0} T_2(\mu) = 0$ such that $|z| \le \gamma_1\lambda$ for all $t \in [T_1(\epsilon) + T_2(\mu), \bar{T})$. Therefore, during time $t \in [T_1(\epsilon) + T_2(\mu), \bar{T})$ $(\eta(t), e(t))$ remains in the set $\Omega_0 \times \Omega_c$, and the variables $(z(t), \zeta(t))$ are bounded by $|z| \le \gamma_1\lambda$, and $\|\zeta\| \le \tilde{\gamma}_2(\epsilon/\mu)$.

Next we analyze (23b) during time $t \in [T_1(\epsilon)+T_2(\mu), \bar{T})$. Note that $(\eta(t), e(t)) \in \Omega_0 \times \Omega_c$ during the time period $[0, \bar{T}]$. Taking the time derivative of V_e along Eq. (23b), which satisfies

$$\begin{aligned} \dot{V}_e &= -e^T Qe + 2e^T PB\{\Gamma[z+\phi](t) - \Gamma[\phi](t)\}, \\ &\le -\lambda_{\min}(Q)\|e\|^2 + 2\lambda k_6\|e\|, \ \forall\ |z| \le \gamma_1\lambda, \end{aligned}$$

where $k_6 = \gamma_1 k\|PB\|$, $\tilde{k} = k + \beta_2$, and $\lambda_{\min}(Q)$ is the minimum eigenvalue of Q, which implies

$$\dot{V}_e \le -\frac{\lambda_{\min}(Q)}{2}\|e\|^2 \quad \text{for } \|e\| \ge \frac{4\lambda k_6}{\lambda_{\min}(Q)}.$$

Therefore, for all $\lambda \le \tilde{\lambda}_1$, where $\tilde{\lambda}_1$ is a small positive constant, $\dot{V}_e < 0$ on the boundary $\{e : V_e(e) = c\}$. Taking $\lambda \le \tilde{\lambda}_1$, ensures that the set $\Omega_0 \times \Omega_c$ is positively invariant. From which we can conclude that $(\eta(t), e(t)) \in \Omega_0 \times \Omega_c$ for all $t \ge 0$, $|z| \le \gamma_1\lambda$ for all $t \ge T_1(\epsilon) + T_2(\mu)$, and $\|\zeta\| \le \tilde{\gamma}_2(\epsilon/\mu)$ for all $t \ge T_1(\epsilon)$. Therefore, there is time $T^*(\lambda_1^*)$, such that for all $t \ge T^*(\lambda_1^*)$, (20) follows. □

5. Simulation results

In this section, a simulation study is conducted to examine the performance of the proposed controller and to highlight the impact of the dynamic inversion parameter μ and the high-gain observer parameter ϵ on the smallness of the tracking error. For simulation purposes, we consider the model for a piezo-actuated nanopositioner, which was identified experimentally and used for the controller design in Esbrook, Tan, and Khalil (2010). It is worth mentioning that the same setup is used later for experimental verification of the proposed controller presented in next section. The model is composed of two cascaded blocks. The first block represents the input hysteresis nonlinearity, modeled by a Modified Prandtl–Ishlinskii (MPI) operator consisting of 8 play operators and 9 deadzone operators. The other block represents the vibrational dynamics, represented as a linear state-space system. The augmented system can be represented as

$$\dot{\xi} = A_\xi\xi + B_\xi\left[\Gamma_\xi[u; v_o](t) + d_\xi(t)\right], \tag{25}$$

where $\xi \in \mathbb{R}^2$ represents the displacement and velocity of the nanopositioning stage, Γ_ξ is the MPI operator with v_o being its initial state, $d_\xi \in \mathbb{R}$ is the input disturbance, and the matrices

$$A_\xi = \begin{bmatrix} 0 & 1 \\ -1.795\times 10^8 & -5696.88 \end{bmatrix} \text{ and } B_\xi = \begin{bmatrix} 0 \\ 1.063\times 10^9 \end{bmatrix}.$$

It should be noted that the model (25) is a special case of the general model (1) in Section 2. Throughout the simulation studies,

Table 1
Simulation results: Mean and Max $|e(t)|\%$ in percent of the reference amplitude in the state feedback case.

μ	Mean $\|e(t)\|\%$	Max $\|e(t)\|\%$
0.1	0.0584	0.0956
0.01	0.0526	0.0895
0.001	0.0119	0.0219
0.0001	0.0012	0.0022

Table 2
Simulation results: Mean and Max $|e(t)|\%$ in percent of the reference amplitude in the output feedback case with $\mu = 0.1$.

ϵ	Mean $\|e(t)\|\%$	Max $\|e(t)\|\%$
0.01	0.2202	0.4512
0.001	0.0609	0.0958
0.0001	0.0607	0.0954
0.00001	0.0602	0.0953

the observer parameters are taken as $\alpha_1 = 3, \alpha_2 = 3$, and $\alpha_3 = 1$, while the controller gain is taken as $K = [2 \;\; 1]$. Moreover, it was assumed that the nanopositioner is initially at a stationary state with position zero at the starting point. A sinusoidal reference is used with frequency of 100 Hz and amplitude of 10 μm. The input disturbance signal d_ξ consists of the 3rd, 5th, and 7th harmonics of the reference signal frequency with amplitudes equal to 1, 0.2, and 0.1, respectively. Table 1 shows the simulation results for the state feedback case, where all system state variables and the hysteretic output are measured. Both the mean and maximum values of the tracking error, normalized by the amplitude of the reference signal (and thus expressed as %), are shown in Table 1, for a range of dynamic inversion parameter μ. As observed clearly, both the mean and maximum errors are reduced significantly when the value of the parameter μ is decreased.

Table 2 shows the simulation results for the output feedback case, where the value of the parameter μ is fixed at 0.1, while the extended high-gain observer parameter ϵ is chosen at a few different values as shown in the table. Note that both the mean and maximum tracking errors are reduced dramatically when the value of ϵ is reduced from 0.01 to 0.001. However, reducing the value of ϵ to lower values only results in slight decrease in the tracking errors, which inch towards the tracking error performance in the state-feedback case for $\mu = 0.1$.

The above simulation results support the major theoretical findings of the ultimate boundedness of the closed-loop system as summarized in both Theorems 1 and 2; in particular, the tracking error can be reduced by decreasing the parameter μ for the state feedback case and $\max(\mu, \frac{\epsilon}{\mu})$ for the output feedback case, respectively.

6. Experimental results

To further verify the theoretical results, a series of tracking experiments are conducted on a commercial nanopositioner (Nano OP-65, from Mad City Labs). The data acquisition and control are realized through dSPACE (DS1104). Three types of reference signals are used in the experiments, including sinusoidal signals, sawtooth signals, and multi-harmonic signals. The observer and the controller parameters used in the experiments are $\alpha_1 = 3$, $\alpha_2 = 3$, $\alpha_3 = 1$, $\mu = 0.01$, $\epsilon = 6.6667 \times 10^{-6}$, and $K = [2, 1.3398 \times 10^4]$. To mitigate the effect of noise amplification due to the use of high-gains in the observer, a low-pass filter with 1 KHz bandwidth is inserted at the measurement side.

In the experiments we have used four different sinusoidal signals with frequencies of 5, 25, 50, 100 Hz, respectively. The experimental results for the highest reference frequency, i.e., 100 Hz, are shown in Fig. 1. As can be seen in Fig. 1(a), the measured position output converges to the reference signal at roughly 0.009 s, which is shown more clearly in Fig. 1(b). Moreover, it can be seen in the magnified part of Fig. 1(b) that the tracking error at the steady state is within ±0.055 μm.

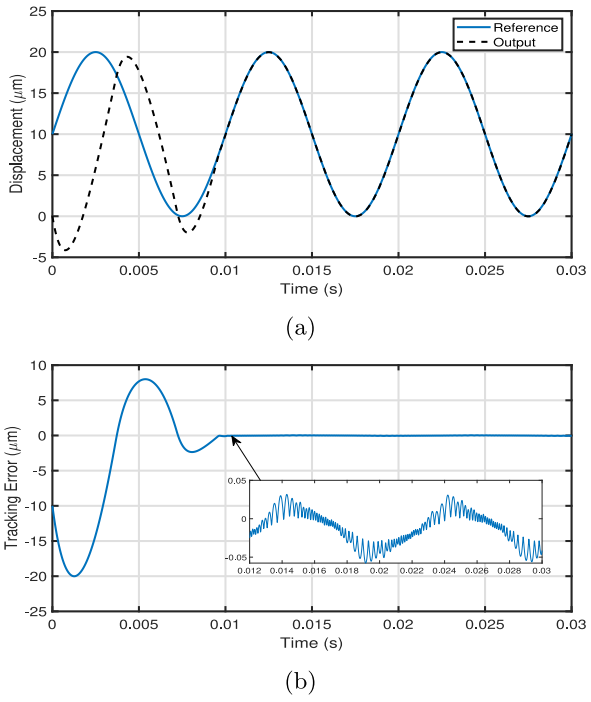

Fig. 1. Experimental results on tracking a 100 Hz sinusoidal reference signal. (a) Positioner displacement; (b) tracking error.

Table 3
Experimental results: Comparison of the Mean $|e(t)|\%$ in tracking a sinusoidal reference.

Frequency	EHGO-DI	SMC	SHSC	MHSC	PI
5 Hz	0.1343	0.1190	0.6490	0.2710	0.5141
25 Hz	0.1330	0.6200	0.7070	0.2680	0.5540
50 Hz	0.1371	0.6600	0.7700	0.2840	0.6286
100 Hz	0.2051	0.8300	0.8150	0.3520	0.8242

Tables 3 further provides a comparison of the mean percentage tracking error performance between the proposed controller (EHGO-DI) and several competing controllers, including a sliding mode controller (SMC) with hysteresis inversion in Edardar et al. (2015), a single-harmonic servocompensator (SHSC) (Esbrook et al., 2013), a multiple-harmonic servocompensator (MHSC) (Esbrook et al., 2013), and a proportional–integral controller implemented solely without using feedforward inversion. Note that hysteresis inversion is used in both SHSC and MHSC (Esbrook et al., 2013). It can be seen that, overall the proposed controller outperforms all the other approaches. In Table 3, it can be noticed that our proportional–integral controller is comparable to the SHSC controller and it does slightly better than the SMC approach.

The next set of experiments are implemented with sawtooth reference signals with frequencies of 5, 25, 50, and 100 Hz, respectively. To avoid impulsive behavior, a second-order linear filter is utilized to smooth out the signal edges. Figs. 2(a) and 2(b) show the time trajectories of the positioner displacement and the tracking error for the 100 Hz case, where it can be seen that the displacement converges to the reference signal at roughly 0.003 s. Note that the tracking error is confined to around ±0.05 μm at the steady state. The first part of Table 4 shows the

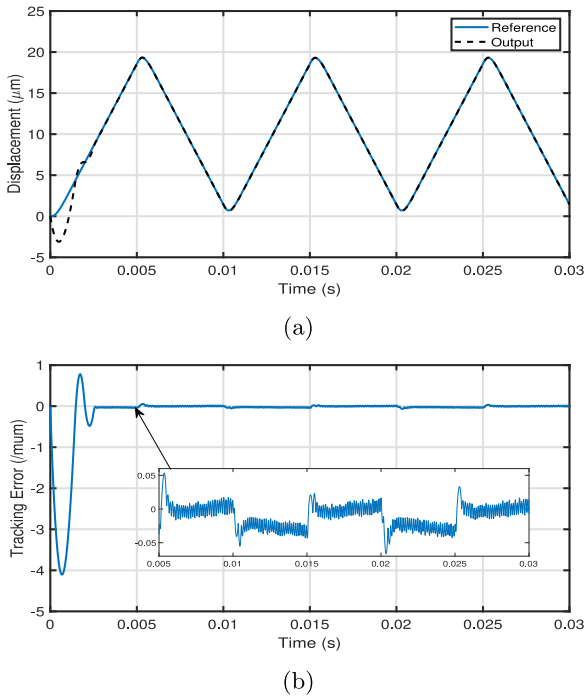

Fig. 2. Experimental results on tracking a 100 Hz sawtooth reference signal. (a) Positioner displacement; (b) tracking error.

Table 4
Experimental results: Mean and Max $|e(t)|\%$ in percent of the reference amplitude for sawtooth and Multi-Harmonic references.

Frequency	sawtooth		Multi-Harmonic	
	Mean $\|e(t)\|\%$	Max $\|e(t)\|\%$	Mean $\|e(t)\|\%$	Max $\|e(t)\|\%$
5 Hz	0.1354	0.2355	0.1389	0.2440
25 Hz	0.1358	0.3422	0.1397	0.3063
50 Hz	0.1401	0.5388	0.1496	0.4671
100 Hz	0.1893	0.8905	0.2486	0.9744

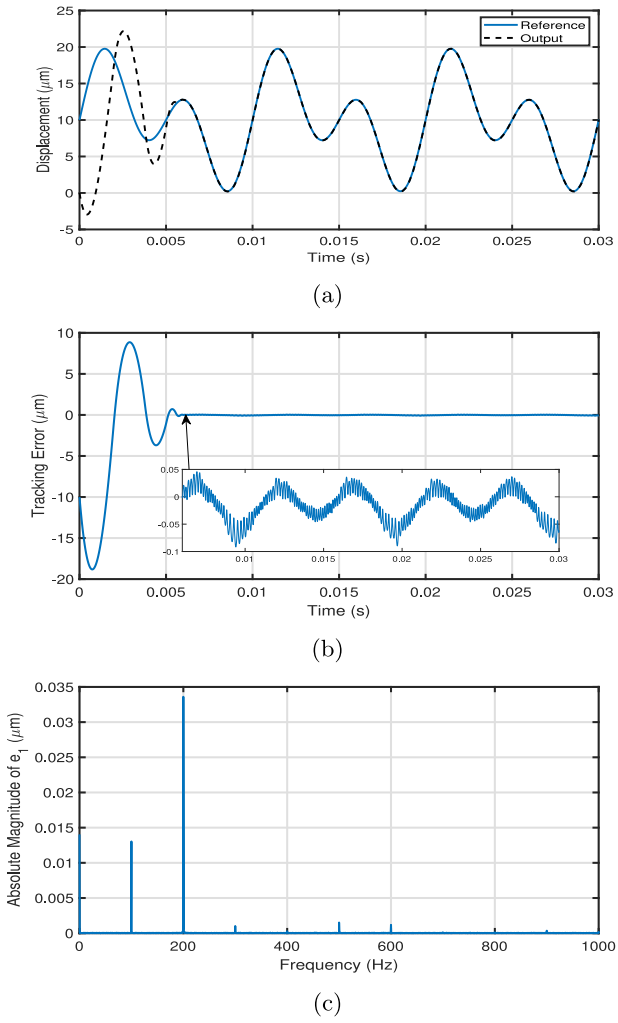

Fig. 3. Experimental results on tracking a multi-harmonic reference with a primary frequency of 100 Hz. (a) Positioner displacement; (b) tracking error; (c) frequency spectrum of the tracking error.

mean and maximum tracking errors over the considered range of frequencies.

In the final set of experiments, the tracking of a multi-harmonic signal with first and second harmonics is implemented. Similar to the previous experiments, we consider a range of primary frequencies, $5, 25, 50, 100$ Hz. As seen from Figs. 3(a) and 3(b), the positioner output converges to the reference signal in roughly 0.006 s. The tracking error at the steady state is larger than the two previous cases (sinusoidal and sawtooth references). Fig. 3(c) also shows the amplitudes of the 1st and 2nd harmonic components of the error. It can be noticed that the absolute amplitude of the 2nd harmonic is larger than the 1st one. The second half of Table 4 shows quantitative results on the tracking error for all frequencies. Overall the results are satisfactory; the tracking errors are slightly larger comparing to the smoothed sawtooth case. This can be attributed to the pronounced 2nd harmonic component in the reference signal.

7. Conclusion

This paper presented a novel hysteresis compensation algorithm using dynamic inversion and extended high-gain observer. While many of the state-of-the-art methods for hysteresis compensation require the construction of (often times) computation-intensive inverse hysteresis model, the proposed approach does not require such an explicit inverse. In addition, the controller is robust with respect to the system uncertainties and does not require the exact knowledge of the plant parameters. This is because such uncertainties can be combined with the hysteresis output in the signal σ, which is estimated by the extended high-gain observer. The mild assumption on the hysteresis nonlinearity is easily satisfied by popular hysteresis operators like the classical PI operator, the generalized PI operator and the KP operator. This work, to our best knowledge, is the first to extend the dynamic inversion theory to the case of hysteretic systems with rigorous analysis. The approach was further validated with simulation and extensive experimental evaluation. The experiments on a nanopositioner confirm the effectiveness of the proposed control scheme and demonstrate comparable tracking performance with the aforementioned algorithms. For future work, we will explore the application of the proposed approach in other smart material-actuated systems.

Acknowledgment

The authors would like to thank Prof. Hassan K. Khalil for his valuable input on this work.

References

Al Janaideh, M., & Boker, A. M. (2018). *Modeling and output-feedback control of systems with Netushil rate-dependent hysteresis nonlinearties* (pp. 6912–6917). IEEE.

Bashash, S., & Jalili, N. (2009). Robust adaptive control of coupled parallel piezo-flexural nanopositioning stages. *IEEE/ASME Transactions on Mechatronics*, *14*(1), 11–20.

Bertotti, G., & Mayergoyz, I. D. (2006). *The science of hysteresis III*. Oxford: Academic Press.

Bouc, R. (1967). Forced vibration of mechanical systems with hysteresis.

Brokate, M., & Sprekels, J. (2012). *Hysteresis and phase transitions (Vol. 121)*. Springer Science & Business Media.

Chen, X., Hisayama, T., & Su, C.-Y. (2009). Pseudo-inverse-based adaptive control for uncertain discrete time systems preceded by hysteresis. *Automatica*, *45*(2), 469–476.

Chen, X., Hisayama, T., & Su, C.-Y. (2010). Adaptive control for uncertain continuous-time systems using implicit inversion of Prandtl-Ishlinskii hysteresis representation. *IEEE Transactions on Automatic Control*, *55*(10), 2357–2363.

Chen, J., Ren, B., & Zhong, Q.-C. (2015). Hysteresis compensation in piezoelectric actuator positioning control based on the uncertainty and disturbance estimator. In *2015 American control conference* (pp. 2537–2542). IEEE.

Chowdhury, D., Al-Nadawi, Y. K., & Tan, X. (2018). Hysteresis compensation using extended high-gain observer and dynamic inversion. In *ASME 2018 dynamic systems and control conference* (p. V002T24A005). American Society of Mechanical Engineers.

Devasia, S., Eleftheriou, E., & Moheimani, S. O. R. (2007). A survey of control issues in nanopositioning. *IEEE Transactions on Control Systems Technology*, *15*(5), 802–823.

Edardar, M., Tan, X., & Khalil, H. K. (2015). Design and analysis of sliding mode controller under approximate hysteresis compensation. *IEEE Transactions on Control Systems Technology*, *23*(2), 598–608.

Esbrook, A., Tan, X., & Khalil, H. K. (2010). A robust adaptive servocompensator for nanopositioning control. In *49th IEEE conference on decision and control* (pp. 3688–3693).

Esbrook, A., Tan, X., & Khalil, H. K. (2013). Control of systems with hysteresis via servocompensation and its application to nanopositioning. *IEEE Transactions on Control Systems Technology*, *21*(3), 725–738.

Filippov, A. F. (2013). *Differential equations with discontinuous righthand sides: Control systems (Vol. 18)*. Springer Science & Business Media.

Freidovich, L. B., & Khalil, H. K. (2008). Performance recovery of feedback-linearization-based designs. *IEEE Transactions on Automatic Control*, *53*(10), 2324–2334.

Goforth, F. J., & Gao, Z. (2008). An active disturbance rejection control solution for hysteresis compensation. In *2008 American control conference* (pp. 2202–2208). IEEE.

Hovakimyan, N., Lavretsky, E., & Sasane, A. (2007). Dynamic inversion for nonaffine-in-control systems via time-scale separation, Part I. *Journal of Dynamical and Control Systems*, *13*(4), 451–465.

Janaideh, M. A., Rakheja, S., & Su, C. Y. (2011). An analytical generalized Prandtl–Ishlinskii model inversion for hysteresis compensation in micropositioning control. *IEEE/ASME Transactions on Mechatronics*, *16*(4), 734–744.

Khalil, H. K. (2002). *Nonlinear systems (Vol. 3)*. Upper Saddle River, NJ: Prentice hall.

Khalil, H. K. (2017). *High-gain observers in nonlinear feedback control*. Philadelphia, PA: Society for Industrial and Applied Mathematics.

Krasnosel'skiĭ, M. A., & Pokrovskiĭ, A. V. (1989). *Systems with hysteresis*. Springer.

Krejci, P., & Kuhnen, K. (2001). Inverse control of systems with hysteresis and creep. *IEE Proceedings D (Control Theory and Applications)*, *148*(3), 185–192.

Kuhnen, K. (2003). Modeling, identification and compensation of complex hysteretic nonlinearities: A modified Prandtl-Ishlinskii approach. *European Journal of Control*, *9*(4), 407–418.

Leang, K. K., Zou, Q., & Devasia, S. (2009). Feedforward control of piezoactuators in atomic force microscope systems. *IEEE Control Systems Magazine*, *29*(1), 70–82.

Lee, J., Mukherjee, R., & Khalil, H. K. (2016). Output feedback performance recovery in the presence of uncertainties. *Systems & Control Letters*, *90*, 31–37.

Mayergoyz, I. D. (2003). *Mathematical models of hysteresis and their applications*. Academic Press.

Oh, J., & Bernstein, D. S. (2005). Semilinear Duhem model for rate-independent and rate-dependent hysteresis. *IEEE Transactions on Automatic Control*, *50*(5), 631–645.

Oh, S., & Khalil, H. K. (1995). Output feedback stabilization using variable structure control. *International Journal of Control*, *62*(4), 831–848.

Paden, B., & Sastry, S. (1987). A calculus for computing Filippov's differential inclusion with application to the variable structure control of robot manipulators. *IEEE Transactions on Circuits and Systems*, *34*(1), 73–82.

Ruderman, M., & Bertram, T. (2010). Discrete dynamic preisach model for robust inverse control of hysteresis systems. In *49th IEEE conference on decision and control* (pp. 3463–3468). IEEE.

Ruderman, M., & Rachinskii, D. (2018). Discrete-time adaptive hysteresis filter for parallel computing and recursive identification of preisach model. In *2018 IEEE conference on control technology and applications* (pp. 1096–1101). IEEE.

Tan, X., & Baras, J. S. (2004). Modeling and control of hysteresis in magnetostrictive actuators. *Automatica*, *40*(9), 1469–1480.

Tao, G., & Kokotovic, P. V. (1995). Adaptive control of plants with unknown hystereses. *IEEE Transactions on Automatic Control*, *40*(2), 200–212.

Wang, Q., & Su, C.-Y. (2006). Robust adaptive control of a class of nonlinear systems including actuator hysteresis with Prandtl–Ishlinskii presentations. *Automatica*, *42*(5), 859–867.

Webb, G. V., Lagoudas, D. C., & Kurdila, A. J. (1998). Hysteresis modeling of sma actuators for control applications. *Journal of Intelligent Material Systems and Structures*, *9*(6), 432–448.

Yi, J., Chang, S., & Shen, Y. (2009). Disturbance-observer-based hysteresis compensation for piezoelectric actuators. *IEEE/ASME Transactions on Mechatronics*, *14*(4), 456–464.

Dhrubajit Chowdhury received the B.Tech. degree in Electronics and Communication Engineering from Jalpaiguri Govt. Engg. College, India, in 2013 and the M.Tech. degree in Mechatronics from AcSIR, India, in 2015. He completed his Ph.D. degree in Electrical and Computer Engineering at Michigan State University, East Lansing, MI, USA in August, 2020.

He received the People's Choice award in the Three Minute Thesis Competition at the Graduate Academic Conference at Michigan State University. He is also the recipient of the 2019–20 Fitch H. Beach award for the most outstanding graduate researcher in the Electrical and Computer Engineering Department at Michigan State University. His research interests include control of multi-agent systems, output feedback control of nonlinear systems, anomaly detection using data science, and optimization of desalination systems.

Yasir K. Al-Nadawi received his Ph.D. degree in electrical engineering focused on controls in 2021 from Michigan State University, East Lansing, MI, USA. He received his M.Sc. degree in control and systems engineering from the University of Technology, Baghdad, Iraq, in 2008 and his B.Sc. from the same university, in 2005. Currently, he is an Automated Vehicle Controls research engineer with Honda research institute (US), Ann Arbor, MI. His research interests include nonlinear control systems design and analysis, in particular multi-time-scales approaches, singular perturbation theory, sliding mode control theory, disturbance observers, and regulation Theory. On the application side, he is interested in vehicle dynamics and control, autonomous driving, cooperative control, electrified powertrain control applications, and energy efficiency.

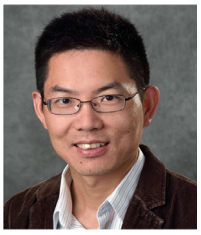

Xiaobo Tan received the B.Eng. and M.Eng. degrees in automatic control from Tsinghua University, Beijing, China, in 1995 and 1998, respectively, and the Ph.D. degree in electrical engineering from the University of Maryland, College Park, in 2002. He is currently an MSU Foundation Professor and the Richard M. Hong Endowed Chair in the Department of Electrical and Computer Engineering (ECE) at Michigan State University (MSU). His research interests include control systems, smart materials, underwater robotics, and soft robotics.

Dr. Tan is a Senior Editor for IEEE/ASME Transactions on Mechatronics. He has coauthored over 250 peer-reviewed journal and conference papers, and holds four US patents. He is a Fellow of IEEE and ASME, and a recipient of NSF CAREER Award (2006), MSU Teacher-Scholar Award (2010), MSU College of Engineering Withrow Distinguished Scholar Award (2018), Distinguished Alumni Award from the ECE Department at University of Maryland (2018), and multiple best paper awards.